EFFECT OF CLOSURE CONFINEMENT ON HORIZONTAL CONVECTION

Sajjad Hossain, Tony Vo, and Gregory J. Sheard

The Sheard Lab, Department of Mechanical and Aerospace Engineering, Monash University, VIC 3800, Australia

ABSTRACT

Horizontal convection is investigated numerically in shallow rectangular enclosures with height-to-length aspect ratios up to 160 times shallower than has been studied previously to determine the effect of ocean-relevant confinement on horizontal convection. Simulations are performed at a Prandtl number of $Pr = 6.14$ (consistent with water) across a wide span of Rayleigh numbers, ($10 \leq Ra \leq 10^{16}$) and aspect ratios ($10^{-3} \leq A = H/L \leq 0.16$). The Boussinesq flow is driven by imposing a linear temperature variation from colder to warmer across the bottom boundary of the enclosure, and insulating temperature conditions on the remaining boundaries.

This work, for the first time, focuses on the effect of aspect ratio towards the shallow-enclosure limit. A critical Ra has been identified marking the transition between the diffusion-dominated and convective regimes. The heat transfer scalings within these regimes are determined as a function of aspect ratio and Nusselt number, Nu. These scalings provide evidence that at lower Ra, the height of the enclosure controls the flow dynamics, and modified Nu and Ra have been defined. The velocity and temperature solutions in this regime display self-similarity features that are described by analytical solutions of one-dimensional channel flow. This result provides further evidence that horizontal convection flow in shallow enclosures resembles one-dimensional channel flow at low Ra, away from the end-walls.

1 INTRODUCTION

Horizontal convection is a distinctive mode of convective heat transfer where heating and cooling occurs along the same horizontal boundary. In contrast to the substantially studied Rayleigh–Bénard convection, where convective overturning circulation is stimulated by both heating and cooling, the strength of overturning in horizontal convection is ultimately limited by heat diffusion [1]. The inspiration for research in horizontal convection originates from its relevance to geophysical flows and process engineering [2].

Several studies regarding horizontal convection have been performed in both numerical and experimental aspects to investigate the flow dynamics. Experiments by Mullarney et al. [3] with water in an enclosure of aspect ratio, A=0.16 (height to length) showed that beyond the diffusion-dominated regime, the Nusselt number scales approximately with $Ra^{1/5}$, which is similar to the Rossby scaling [4]. Chiu-Webster et al. [5] studied horizontal convection in the infinite-Prandtl number limit relevant to very viscous fluids at a range of A and Ra with highest values of 2 and 10^{10}, respectively. The authors also recovered the Rossby scaling of $Nu \propto Ra^{1/5}$, and provided evidence of aspect ratio independence of this scaling for $Ra > 10^7$. However, Siggers et al. [6] used a variational analysis to report a higher upper bound of the scaling, namely $Nu \propto Ra^{1/3}$. Sheard and King [7] used a spectral element method to investigate horizontal convection for aspect ratios, $0.16 \leq A \leq 2.0$ at a range of Rayleigh and fixed Prandtl number representative of water ($Pr = 6.14$). They reported an aspect ratio dependence feature the measured Nu and boundary layer thickness at low Ra. The authors also confirmed an increase in the exponent of Ra 1/5th to 1/3rd in the convective regime for the Nu scaling. This uplift was later shown to represent a shift between flow regimes both obeying $Nu \propto Ra^{1/5}$ [8].

Despite horizontal convection being strongly motivated by a desire to understand the role of buoyancy forcing in global ocean currents, it is evident that the previously investigated range of enclosure aspect ratios ($A \geq 0.16$) is well above ocean-relevant values ($10^{-5} \leq O(A) \leq 10^{-3}$). Therefore, this study aims to provide insights into horizontal convection, its regimes, and the scalings of significant quantities towards the limit of shallow aspect ratios.

2 METHODOLOGY

The computation domain comprises a rectangular fluid-filled enclosure with water, having internal dimensions of length L, height, H (aspect ratio, $A = H/L$). The flow is driven by a linear temperature profile applied along the bottom wall of the enclosure, as shown in figure 1. The side and top walls are thermally insulated (a zero wall-normal temperature gradient is imposed), and a no-slip condition is imposed on the velocity field on all walls. The buoyancy is modelled with the Boussinesq approximation, which implies that the density differences in the fluid are disregarded except for the contribution of gravity. Hence, the energy equation simplifies to a scalar advection

diffusion equation for temperature, which is evolved in accordance with the velocity field.
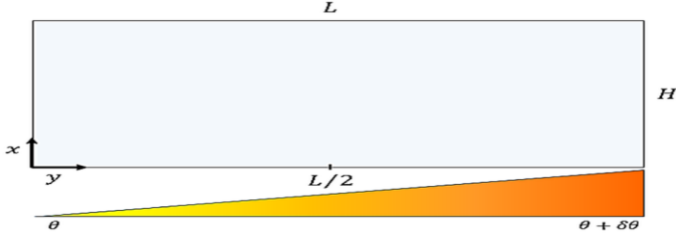

Figure 1: A schematic diagram of the system. The origin of the coordinate system placed at the bottom-left corner, and a temperature difference of δθ imposed along the bottom boundary.

The fluid temperature is related linearly to the density via thermal expansion coefficient α. The Navier–Stokes equations governing a Boussinesq fluid are written as

$$\frac{\partial \mathbf{u}}{\partial t} = -(\mathbf{u} \cdot \nabla)\mathbf{u} - \nabla p + Pr\nabla^2 \mathbf{u} - PrRa\hat{g}\theta, \qquad (1)$$

$$\nabla \cdot \mathbf{u} = 0, \qquad (2)$$

$$\frac{\partial \theta}{\partial t} = -(\mathbf{u} \cdot \nabla)\theta + \nabla^2 \theta, \qquad (3)$$

where t is time, θ is the temperature, p is the pressure, $\mathbf{u}$ denotes the velocity vector and $\hat{g}$ is a unit vector in the direction of the gravity. In the governing equations, lengths, time, velocity, pressure and temperature difference are respectively scaled by L, L^2/κ, κ/L, $\rho_\circ \kappa^2 /L^2$ and δθ. The 2D incompressible Navier–Stokes equations augmented by a buoyancy term in the momentum equation and a scalar advection-diffusion transport equation for temperature are solved by a high-order in-house solver, which employs a spectral-element method for spatial discretisation and a 3rd-order time integration scheme based on backwards-differencing.

Meshes are constructed for various aspect ratios from $A = 0.16$ down to 0.001. The number of spectral elements in the meshes varies between 296 and 4128. The elements are concentrated in the vicinity of the side walls; and adjacent to the hot bottom end boundary to ensure that flow is resolved, while relaxing the mesh density in the interior. The highest aspect ratio considered in this study (0.16) corresponds to the lowest aspect ratio previously considered in the literature. After a thorough grid resolution study, a polynomial order of 5 was selected to conduct the study considering a trade-off between computational cost and accuracy.

3 RESULTS AND DISCUSSION

The Nusselt number is calculated from the obtained flux values along the bottom horizontal boundary of the enclosure for each aspect ratio configuration, and these are plotted against the Rayleigh number in figure 2. Nusselt number is found to be directly proportional to the aspect ratios ($Nu \propto A$) and independent of Rayleigh number at low Rayleigh numbers: this range of Rayleigh numbers is identified as the diffusion-dominated or conduction regime. With an increase in Rayleigh number, the Nusselt number for all aspect ratios demonstrate a rapid rise in the transition regime before collapsing onto a single line: this region is identified as the convective regime. The results show that by increasing enclosure confinement, i.e. towards smaller aspect ratios, the onset of the transition regimes delays to a higher Rayleigh number. The onset of the transition regime is quantified by introducing a critical value of Rayleigh and Nusselt number for each aspect ratio. A 5% deviation from the Rayleigh-number-independent value of the Nusselt number is taken to mark the critical Rayleigh number. The critical Nusselt and Rayleigh numbers are found to closely fit to power-law scalings having $Ra \propto A^{-4}$ and $Nu \propto Ra^{-1/4}$.
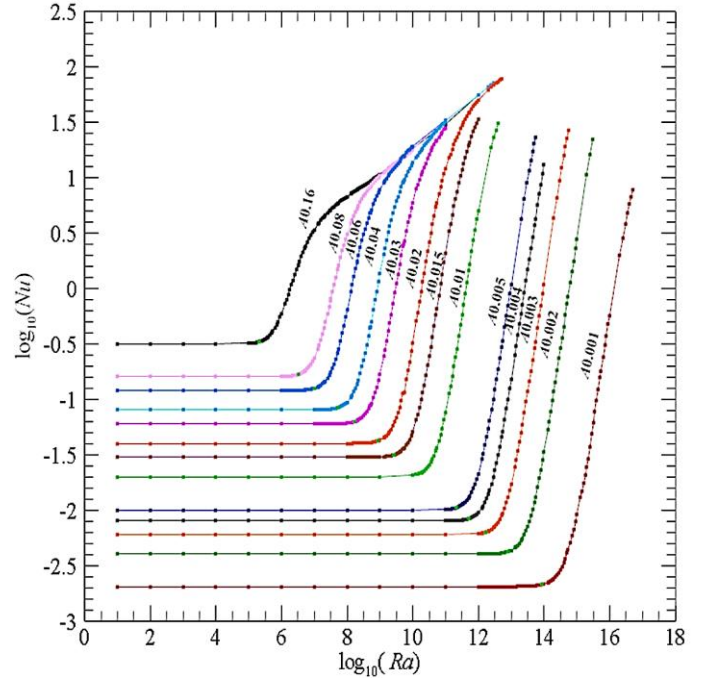

Figure 2: A plot of $\log_{10}(Nu)$ against $\log_{10}(Ra)$ for $0.001 \leq A \leq 0.16$.

Based on the low-Ra/low-A scalings of $Ra \propto A^{-4}$ and $Nu \propto A$, the figure 2 could be rescaled and plotted as Nu / A against $Ra.A^4$, the outcome of which is shown in figure 3. For lower values of $Ra.A^4$, the corresponding values of Nu/A have collapsed into a single line, which is consistent for all aspect ratios. This collapse indicates that the flow in this region is only governed by the height of the enclosure, which may be understood through modified Nusselt and Rayleigh numbers defined as

$$Nu_H = \frac{Nu}{A} = \frac{F_T L}{\rho_\circ C_p \kappa_T (\delta\theta_H)}$$

$$Ra_H = Ra\ A^4\ = \frac{g\alpha(\delta\theta_H)}{\upsilon\kappa_T}H^3$$
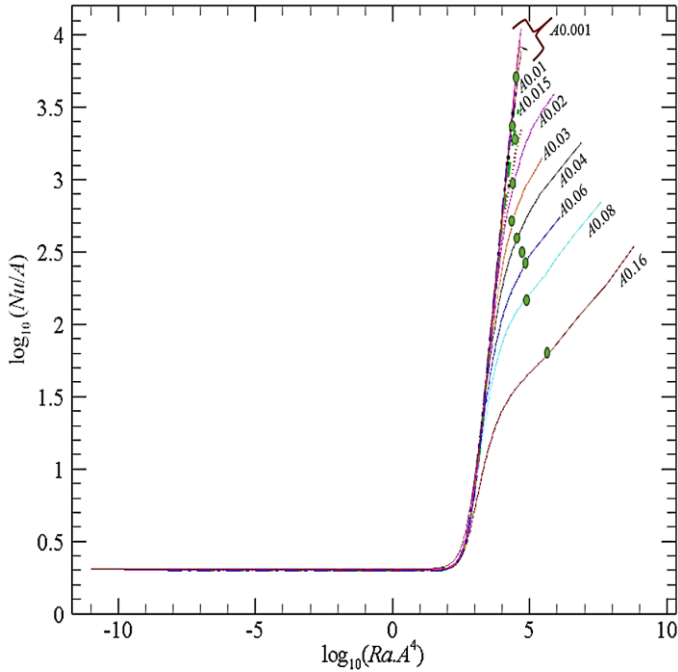

Figure 3: The *Nu-Ra* plot is rescaled with *Ra* $\propto A^{-4}$ and *Nu* $\propto A$ to investigate the self-similarity features. The small green circles on each aspect ratio denotes the onset of unsteady flow.
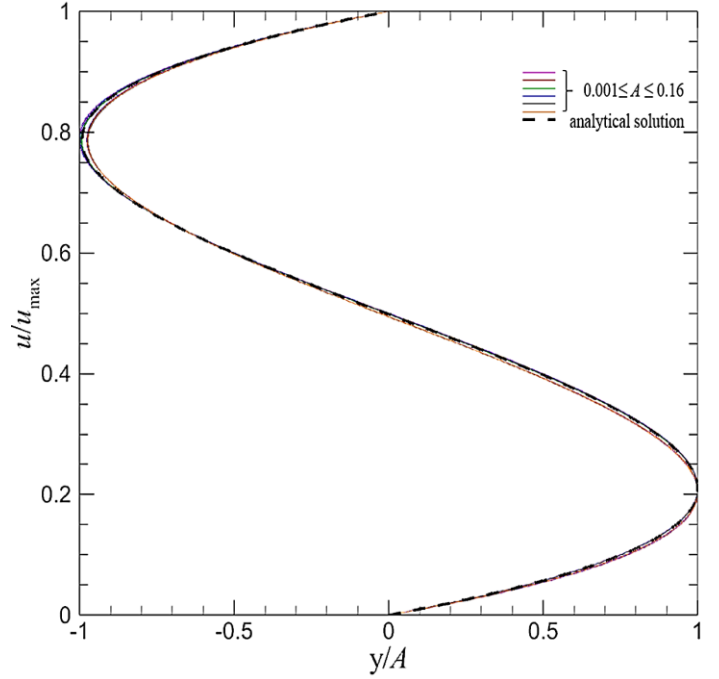

Figure 4: The velocity profiles generated from different locations throughout the horizontal bottom boundary are plotted with the analytical solution.

Here $\delta\theta_H$ is the temperature difference along a portion of the bottom boundary of length H; this appears in both definitions. Additionally, note that L has been replaced by H as the characteristic length quantity appearing in the modified Rayleigh number definition. The corollary to this is that in very shallow enclosures, horizontal convection will be insensitive to the overall length of the enclosure, rather its behaviour will be controlled by the enclosure height and the horizontal temperature gradient acting over that same scale.

Figure 3 shows that beyond the critical Ra_H, Nu/A values for all aspect ratio start branching off from the highest A=0.16 to the lowest A=0.001 with increasing Rayleigh number, which resembles the opposite of the collapse in *Nu-Ra* plot in the convection dominated regime.

Attention is now turned to profiles of the horizontal velocity component extracted at various horizontal locations within the enclosures. The locations are selected for different distances from the hot end, and expressed as a function of the enclosure height. The extracted velocities were normalized by the maximum value from each profile, while the vertical coordinate was normalised by enclosure height. Results are shown in figure 4, which presents the combined velocity profiles for all aspect ratios at a single value of $Ra.A^4$ within the collapsed regime. The

normalized profiles exhibit a strong collapse to a universal profile, implying a self-similarity in the velocity fields in this regime. By observing the extracted velocity data points for all aspect ratios throughout different locations (which are expressed in terms of the distance from the hot-end wall) along the horizontal boundary, it is evident from figure 5 that beyond a distance of approximately $4H$ (the distance from side-wall at the hot end of the enclosure-wall expressed as four times the height of enclosure), all data points consistently demonstrate a collapse to a single value. This demonstrates that the effects of the sidewalls in conduction-dominated horizontal convection are confined to within $4H$ from the wall, and this distance scales with height, not the horizontal enclosure length. Away from these end-wall regions the velocity profile is uniform across the horizontal extent of the enclosure. This behavior will emerge in enclosures having $L > 8H$, or $A = H/L < 1/8$ ($A < 0.125$), which is shallower than the shallowest ($A = 0.16$) enclosure investigated previously.
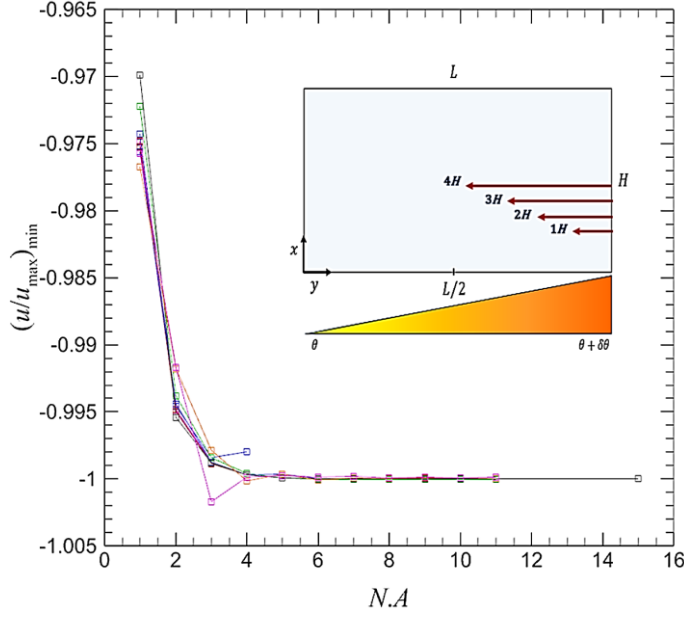
AHMTC11

Figure 5: Minimum values of the scaled velocity plotted with the distance form hot-end wall. The distance is expressed in terms of the integer, N of the aspect ratio of the enclosure. The inset figure demonstrates how the distance from the hot-end represented the integer of aspect ratio.
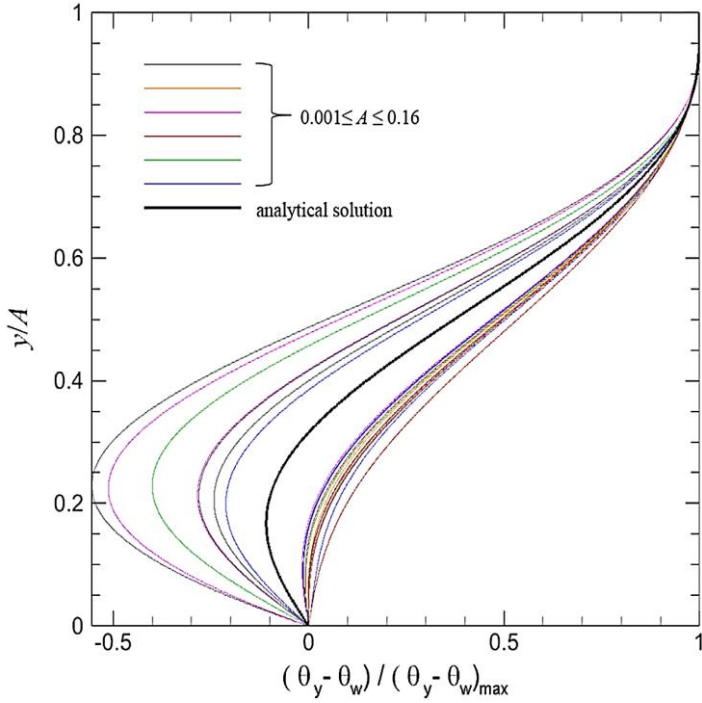

Figure 6: The temperature profiles generated from different locations throughout the horizontal bottom boundary are plotted with the analytical solution.

Similarly, temperature profiles relative to the local bottom wall temperature were extracted and normalized by the vertical temperature difference of each profile. The results are shown in figure 6. In contrast to the velocity contour scaling, the temperature contours for all aspect ratios are not well-collapsed as the obtained values in the vicinity of the hot-end wall seems to deviate from the rest of the data sets. However, similar to the velocity contours, the temperature contours also demonstrate the self-similarity feature beyond the $4H$ distance from the end walls for all aspect ratios.

Polynomial fits to the scaled velocity and temperature profiles are similar to the analytical solution for flow in a horizontal channel driven by a horizontal temperature gradient under a zero net horizontal flow constraint, which is given as

$$U = \frac{\alpha g \beta}{12 \upsilon} (2y^3 - 3hy^2 + h^2 y) \tag{4}$$

$$\theta = \frac{\alpha g \beta^2}{24 \upsilon \kappa} \left(\frac{1}{5} y^5 - \frac{h}{2} y^4 + \frac{h^2}{3} y^3 \right) \tag{5}$$

4. CONCLUSION

Horizontal convection at ocean-relevant shallow enclosures having aspect ratios as small as 160 times shallower than has previously been considered have been investigated by employing high-resolution spectral element simulations with a linear temperature profile applied alongside the horizontal boundary. Modified Rayleigh and Nusselt numbers are proposed for the low-Rayleigh-number conduction-dominated regime. These modified parameters reveal that in shallow enclosures, horizontal convection is controlled not by the enclosure width, but by its height. Furthermore, a previously unseen behaviour is discovered, whereby the turning of the flow at the enclosure sidewalls is confined to a small region near the walls, while away from the walls the flow is horizontally independent. Self-similarity in velocity and temperature profiles is identified in this regime across different aspect ratios, and consistently the sidewall effects are confined to within a distance of approximately four times the enclosure height. This reveals that the shallowest enclosure previously investigated in the literature, the widely studied $A = 0.16$ enclosure, is not sufficiently shallow to capture these effects.

NOMENCLATURE

Greek letters

β =linear temperature gradient along the x-axis

θ = fluid temperature

$\delta\theta$ = temperature difference imposed across

horizontal boundary

κ_T =fluid thermal diffusivity

ν= fluid kinematic viscosity

α= thermal expansion co-efficient

ρ= density of the fluid

$A =H/L$=aspect ratio

g = gravitational acceleration

Nu=Nusselt number

Nu_H = horizontal Nusselt number

P=pressure

Pr= Prandtl number

Ra=Rayleigh number

Ra_H = horizontal Rayleigh number

t=time

u = velocity vector

REFERENCES

1. Hughes, G.O. and R.W. Griffiths, *Horizontal convection.* Annu. Rev. Fluid Mech., 2008. **40**: p. 185-208.
2. Paparella, F., *Turbulence, Horizontal Convection, and the Ocean's Meridional Overturning Circulation*, in *Mathematical Paradigms of Climate Science*. 2016, Springer. p. 15-32.
3. Mullarney, J.C., R.W. Griffiths, and G.O. Hughes, *Convection driven by differential heating at a horizontal boundary.* Journal of Fluid Mechanics, 2004. **516**: p. 181-209.
4. Rossby, H. *On thermal convection driven by non-uniform heating from below: an experimental study*. in *Deep Sea Research and Oceanographic Abstracts*. 1965. Elsevier.
5. Chiu-Webster, S., E. Hinch, and J. Lister, *Very viscous horizontal convection.* Journal of Fluid Mechanics, 2008. **611**: p. 395-426.
6. Siggers, J., R. Kerswell, and N. Balmforth, *Bounds on horizontal convection.* Journal of Fluid Mechanics, 2004. **517**: p. 55-70.
7. Sheard, G.J. and M.P. King, *Horizontal convection: effect of aspect ratio on Rayleigh number scaling and stability.* Applied Mathematical Modelling, 2011. **35**(4): p. 1647-1655.
8. Gayen, B., R.W. Griffiths, and G.O. Hughes, *Stability transitions and turbulence in horizontal convection.* Journal of Fluid Mechanics, 2014. **751**: p. 698-724.